Resonance Microwave Measurements of an Intrinsic Spin-Orbit Coupling Gap in Graphene: A Possible Indication of a Topological State

J. Sichau,[1] M. Prada,[2] T. Anlauf,[1] T. J. Lyon,[3] B. Bosnjak,[1] L. Tiemann,[1] and R. H. Blick[1]
[1]*Center for Hybrid Nanostructures (CHyN), University of Hamburg, Luruper Chaussee 149, 22607 Hamburg, Germany*
[2]*I. Institute for Theoretical Physics, University of Hamburg, Jungiusstrasse 9-11, 20355 Hamburg, Germany*
[3]*Materials Science and Engineering, University of Wisconsin-Madison 1509 Engineering Drive, Madison, Wisconsin 53706, USA*

(Received 14 September 2018; published 1 February 2019)

In 2005, Kane and Mele [Phys. Rev. Lett. **95**, 226801 (2005)] predicted that at sufficiently low energy, graphene exhibits a topological state of matter with an energy gap generated by the atomic spin-orbit interaction. However, this intrinsic gap has not been measured to this date. In this Letter, we exploit the chirality of the low-energy states to resolve this gap. We probe the spin states experimentally by employing low temperature microwave excitation in a resistively detected electron-spin resonance on graphene. The structure of the topological bands is reflected in our transport experiments, where our numerical models allow us to identify the resonance signatures. We determine the intrinsic spin-orbit bulk gap to be exactly 42.2 μeV. Electron-spin resonance experiments can reveal the competition between the intrinsic spin-orbit coupling and classical Zeeman energy that arises at low magnetic fields and demonstrate that graphene remains to be a material with surprising properties.

DOI: 10.1103/PhysRevLett.122.046403

In the early years of the rise of graphene, Kane and Mele [1,2] predicted that the symmetry-allowed spin-orbit potential in graphene gives rise to a spin-Hall insulating (SHI) state [3]. This novel electronic state of matter would be chiral and gapped in the bulk, while supporting spin transport along the sample boundaries. The magnitude of the bulk gap, which is proportional to the atomistic or intrinsic spin-orbit coupling (SOC), determines the observability of an insulator phase of matter that is distinct from any ordinary insulator characterized by chiral states. However, this intrinsic gap has not been experimentally established in graphene to this date, and theoretical controversy exists with regard to its precise magnitude [4–6].

In this Letter, we aim to resolve the intrinsic gap by coupling mesoscopic Hall-bar graphene structures at low temperatures to an external radio-frequency source. We exploit the chirality of the low-energy bands and probe the distinct spin states experimentally by employing microwave excitation in resistively detected electron-spin resonance (RD ESR). We detect two spectral lines of ESR as a function of magnetic field separated by a constant energy. An extended Dirac model allows us to identify this energy separation with the intrinsic SOC gap.

In the Dirac model, the notion of *sublattice spin* is introduced with "up" and "down" states being identified with the two sublattice components u_A^K and u_B^K, respectively, that are centered around atoms of the A and B sublattices [3,7–9]. In the bispinor basis $\{\uparrow,\downarrow\}\otimes\{u_A^K, u_B^K\}$, the effective mass Hamiltonian near the Dirac points (DPs) K and K' takes the form

$$H(\boldsymbol{k},\tau) = \hbar v_F \mathbb{I}_2 \otimes (\tau\sigma_x k_x + \sigma_y k_y) + \lambda_I \tau_z s_z \otimes \sigma_z, \qquad (1)$$

where $\tau = \pm 1$ labels the valley K (K'), σ_i, s_z are the Pauli matrices acting on the sublattice spin and real spin, respectively, $\boldsymbol{k}$ is the coordinate in reciprocal space with a DP at the origin, and $\mathbb{I}_2$ is the unitary 2×2 matrix. The first term yields gapless states with the characteristic linear dispersion of massless Dirac fermions, $E(\boldsymbol{k}) = \pm v_F|\boldsymbol{k}|$. The degeneracy $\boldsymbol{k} = 0$ is protected by sublattice symmetry [3], and elsewhere, $\boldsymbol{\sigma}$ and $\boldsymbol{k}$ are *collinear* and eigenstates of the Hermitian, unitary chirality operator $\hat{h}_k$ [10–14],

$$\hat{h}_k = \boldsymbol{\sigma}\cdot\hat{\boldsymbol{k}}/|\boldsymbol{k}|. \qquad (2)$$

The chirality near K is inverted with respect to the chirality around K' [13–15]. In essence, this dichotomy means that an electron state at K and a hole state at K' are intricately connected by sublattice symmetry [9]. For samples with finite dimensions, this necessarily results in a topological phase, with the emergence of edge states connecting electron and hole bands at different DPs. The second term of Eq. (1) is the effective intrinsic SOC [1–3] and is mostly originated from the poorly occupied d orbitals [16]. This term respects sublattice, parity, and time-reversal symmetries and opens up a bulk gap of opposite sign at each DP of magnitude $|\Delta_I| = 2\lambda_I$. The energetically low-lying edge eigenstates become locally *helical*, with collinear spin $\boldsymbol{s}$ and sublattice spin $\boldsymbol{\sigma}$, as illustrated in Fig. 1(c). The projection of the *chirality* $\hat{h}$ onto the edges is then isomorphic with the Hermitian, unitary *helicity* operator

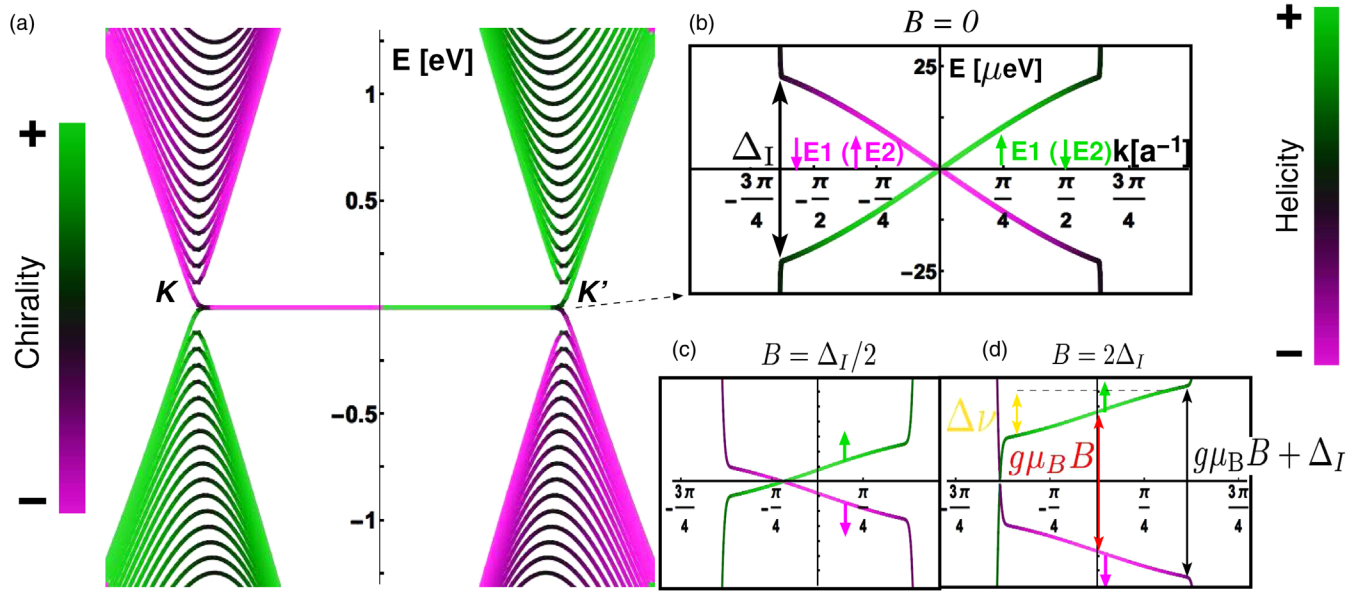

FIG. 1. (a) Band structure of a honeycomb lattice terminated on a zigzag edge with periodic boundary conditions along the armchair direction, colored according to their chirality, $\langle \hat{h}_k \rangle$: Green (magenta) denotes positive (negative) chirality. The states crossing the gap are flat on this energy scale (high DOS). (b) Magnified dispersion relation near the Fermi level of the first Brillouin zone, showing the edge states in detail. The bands are now colored according to their *helicity* $\langle \hat{h}_k \rangle_{\text{edge}}$, with black denoting bulk character. (c),(d) Same as in (b) for the $E1$ bands, with $B = \Delta_I/2$ and $B = 2\Delta_I$, respectively, in units of $g\mu_B$. The spin on each band is indicated with a color matching arrow.

$\langle \hat{h}_k \rangle_{\text{edge}} = 2\langle \hat{\sigma}_z \hat{s}_z \rangle_{\text{edge}}$, where $\langle \ldots \rangle_{\text{edge}}$ means that the evaluation is obtained by projecting onto the edges local density of states (LDOS). In practical terms, this means that the midgap states are spin and sublattice-spin polarized, with the corresponding pseudovectors being either parallel or antiparallel.

Figure 1(a) represents the dispersion of a graphene slab (see Supplemental Material [17]), where the bands are colored according to their chirality $\langle \hat{h}_k \rangle$. In Fig. 1(b), we enlarge the low-lying energy states $E \sim |\Delta_I|$. In order to distinguish the edges from the bulk bands, we color the bands according to their helicity $\langle \hat{h}_k \rangle_{\text{edge}}$, with black denoting now bulklike bands. The bulk shows a gap of $\Delta_I = \pm 2\lambda_I$ of opposite sign at either DP, as expected [27], while the edges are ungapped. Those midgap bands are doubly degenerate pseudospin pairs, with $\sigma_z = \pm 1$, located at either edge. At edge $E1$, the spin-up states have indeed positive velocity, $\partial E/\partial k = v_F^{\text{edge}} > 0$ [green, Fig. 1(b)], whereas those with spin down travel backwards $\partial E/\partial k = -v_F^{\text{edge}} < 0$ [magenta, Fig. 1(b)]. The converse occurs in $E2$, with spin up (down) showing positive (negative) velocity; that is, $E2$ is related to $E1$ by a mirror reflection.

When a magnetic field B is applied perpendicularly to the graphene sheet, the Kramers pairs split into spin-up and -down levels by the Zeeman energy, $g\mu_B B$. In Figs. 1(c) and 1(d) we plot, for clarity, only the midgap $E1$ bands and color them again according to the LDOS. The edge's occupation is maximal at the Γ point, spreading over a bandwidth given by $h\Delta\nu$ [gold double-headed arrows of Fig. 1(d)]. When the Zeeman energy is below the SOC gap, opposite-spin band-crossing pairs occur at the Fermi level and are predominantly localized at either edge [Fig. 1(c)]. The SHI phase is preserved; that is, for the k interval $[0, \pi]$, we encounter an edge state that crosses the Fermi level once for each spin sector. At $g\mu_B|B| > |\Delta_I|$, the SHI is no longer preserved, as the bands at the crossings have bulk character. A gap centered at the Zeeman energy opens between the opposite-spin edge bands [red arrow of Fig. 1(d)].

We address these opposite-spin, helical edge bands by employing RD ESR [28,29], a spin-sensitive probing technique that couples carriers of opposite spin by microwave excitation and detects the response resistively. Our ESR measurements are performed on a Hall-bar graphene structure of 200 μm length and 22 μm width with an intrinsic charge carrier density and mobility of 2×10^{11} cm^{-2} and 3760 cm^2 V^{-1} s^{-1}, respectively [30], at a temperature of $T = 4.2$ K. We minimize the unwanted external SOC sources [6,31,32] and the effective contact area of the graphene with the substrate [29] by suspending the graphene sheet on a trenched SiO_2 layer at zero gate voltage (see Supplemental Material [17]). Microwave excitation is applied through a loop antenna next to the sample (see Fig. 2). The longitudinal sample resistance R_{xx} is then probed as a function of the magnetic field B, both in the absence ($R_{xx,\text{dark}}$) and in the presence ($R_{xx,\nu}$) of microwave radiation. Illuminating the sample reduces the overall resistance, as more conducting bands become populated. Moreover, a

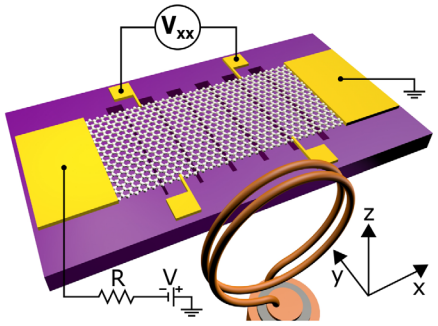

FIG. 2. Schematics of the measurement setup with monolayer graphene patterned into a Hall-bar structure. A nearby loop antenna excites the system (not to scale).

signal in the photoinduced differential resistance $\Delta R_{xx}(\nu) = R_{xx,\mathrm{dark}} - R_{xx,\nu}$ is expected whenever the carrier Zeeman splitting matches the microwave energy of the bulk $h\nu = (2\lambda_I \pm g\mu_B B)$ or that of the edges $h\nu = \pm g\mu_B B$, as dictated by spin selection rules [black and red double-headed arrows of Fig. 1(d), respectively]. At these matching frequencies, the band population increases and the resistance is consequently reduced, revealing a peak in $\Delta R_{xx}(\nu)$ [29]. We emphasize that unlike ideal infinite graphene, a finite DOS exists near the charge neutrality point that originates from edge states (note their rather flat dispersion in Fig. 1). Because of unintentional doping, the Fermi energy is then only shifted by $\Delta E_F \simeq 0.1$ meV (see Supplemental Material [17]), an amount comparable to $k_B T$, and thus allowing a finite amount of thermally excited carriers even within the gap, $f(\Delta_I) = (1 + e^{\Delta E_F/k_B T})^{-1} \gtrsim 0.06$. On the other hand, the Maxwell-Boltzmann distribution dictates $n_\uparrow/n_\downarrow = e^{-g\mu_B B/k_B T} \simeq 0.9$ for $g\mu_B|B| \simeq \Delta_I$, allowing for a detectable signal by net energy absorption even at energies comparable to the intrinsic gap [33].

In Fig. 3(a), $\Delta R_{xx}(\nu)$ is plotted for multiple frequencies, exhibiting a linear dependence of the resonance frequency in magnetic field. Figure 3(b) shows the derivative of $\Delta R_{xx}(\nu)$ in the frequency-magnetic field plane. The two salient "V"-shaped features are separated by a constant frequency of $\nu \approx 10.2$ GHz (42.2 μeV). We stress that due to the extreme flatness of the bands, excitations are allowed within an energetic interval $g\mu_B B + \Delta_I$, which gives rise to positive peaks in $\Delta R_{xx}(\nu)$ as shown in Figs. 1 and 3(a).

The extrapolation of the prominent lower feature intersects with the axis at its origin, representing the edge's Zeeman splitting. When the Zeeman splitting is smaller than the intrinsic gap, the edge states cover the entire range of energies within Δ_I [Figs. 1(c) and 1(d)], as the bands of opposite spin cross at the Fermi energy. However, as the Zeeman splitting overcomes the intrinsic gap, a band of forbidden energies opens up for the edges, allowing an ESR signal to be detected [solid red arrows in Fig. 1(d)]. This is reflected in the strong signal for $|B| \gtrsim |\Delta_I|/g\mu_B$ and in the absence of signal otherwise, which is evidence of the SHI.

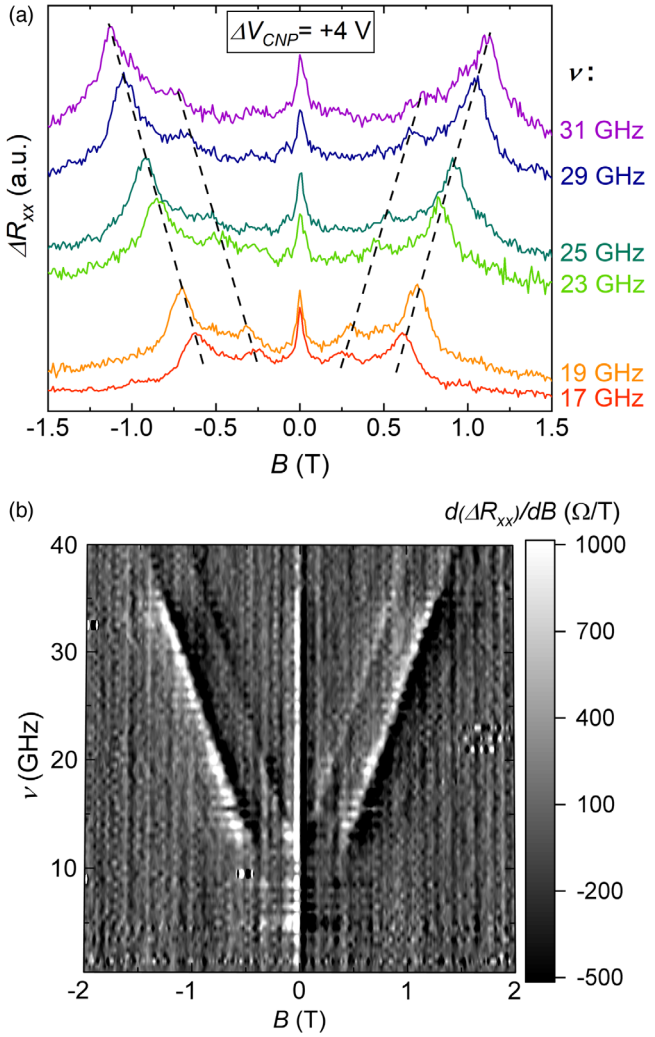

FIG. 3. (a) Individual measurements at $T = 4.2$ K for various frequencies with constant gate voltage $\Delta V_{\mathrm{CNP}} = V_g - V_{\mathrm{CNP}} = 4$ V. Two resonances which are symmetric in B exhibit a linear dependence on ν (dashed lines). The feature at zero field stems from the weak localization in the sample. The data have been shifted and scaled for clarity. (b) Derivative data of all measurements recorded for $0.5\ \mathrm{GHz} \leq \nu \leq 40\ \mathrm{GHz}$. The resonance signal is present over a wide range of frequencies except for $\nu \lesssim 11$ GHz. The upper V feature intercepts the frequency axis at $\nu_1 = 10.2$ GHz, while the lower feature interpolates to $\nu_2 = 0$. This difference corresponds to an energy of $\Delta E = 42.2$ μeV.

The large intensity of the signal is related to the large DOS of the edges, and its width $\Delta\nu$ is related to their dispersive character [see Fig. 1(d)].

We identify the upper V feature with the bulk signal, $h\nu = (\Delta_I \pm g\mu_B B)$ [black double-headed arrows of Fig. 1(c)]. It reveals a zero-field splitting, which is a direct measurement of the *intrinsic* SOC splitting Δ_I: $\nu(B = 0) = (10.2 \pm 0.2)$ GHz, and in energy $\Delta E = (42.2 \pm 0.8)$ μeV. Its weaker intensity reflects the lower DOS of the *bulk*. Moreover, our value is consistent with a zero-field splitting of 10.76 GHz reported by Mani *et al.* [28] on three small,

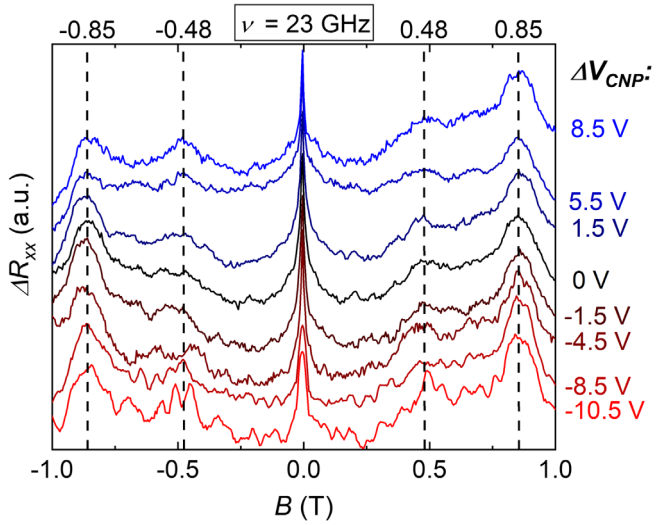

FIG. 4. Individual measurements at $T = 1.4$ K for various gate voltages ΔV_{CNP} with constant frequency $\nu = 23$ GHz, with red (blue) indicating electron (hole) character of the main charge carriers. The two symmetric resonance peaks are evident at $|B_1| = 0.48$ T and $|B_2| = 0.85$ T (dashed lines), and their positions are invariant to gate voltage, i.e., to charge carrier density and type. The data have been shifted and scaled for clarity.

epitaxially grown graphene samples on SiC substrate. The authors did not identify the intrinsic gap to be responsible for their observations; however, their coincident results strongly support our claim: The zero-field splitting corresponds to an *intrinsic* property of graphene, namely, its intrinsic SOC gap, which makes it a sample independent effect. We emphasize that according to Ref. [34], the weak localization peak indicates the strength of the intervalley coupling. The possible splitting of the sublattice degeneracy, which was suggested in Ref. [28], is driven by intervalley scattering. Since intervalley scattering would be sample dependent and sensitive to density, it can be ruled out.

These measurements have been reproduced under different conditions of temperature and carrier densities and in different samples. Figure 4 shows the data for a 1 mm × 100 μm graphene Hall bar on a flat SiO_2 substrate at a temperature of 1.4 K. The two pairs of resonances occur at the same magnetic fields as for the sample of Fig. 3, and their positions are found to be invariant over a wide range of gate voltages. This excludes other possible zero-field splitting candidates, as, e.g., Rashba $H_R = \lambda_R(\boldsymbol{s} \otimes \boldsymbol{\sigma})\hat{z}$ [16,31]. We note that including H_R leaves indeed the SHI picture invariant as long as $\lambda_R < \lambda_I$ [1,2] (see also the Supplemental Material [17]). Finally, we note that for the large sample dimensions we consider in this work, we can safely assume that the edge and bulk signals are width insensitive: Localized solutions for other edge types, such as armchair or ragged edges, yield qualitatively similar results due to the bulk-edge correspondence and the continuum limit [35].

The magnitude of the intrinsic gap in graphene determines the observability of the SHI phase but has been the subject of theoretical controversy: After its initial rough estimate of about 100 μeV by Kane *et al.* [2], Min *et al.* [4] and Yao *et al.* [5] reported independently a theoretical calculation of 1 μeV. Konschuh *et al.* [6] and Boettger and Trickey [36] used first-principles calculations to deliver a larger value, around the 25–50 μeV. Our experimental measurement agrees best with this range, rendering the SHI experimentally accessible for graphene.

In graphene, the symmetry protected sublattice degeneracy favors the emergence of a fascinating state of matter, the SHI. We find its presence encoded in exotic transitions that can be observed in RD ESR experiments. To illuminate the origin of these ESR transitions and the underlying complex band structure in suspended graphene, we have employed the conventional Dirac model and characterized the bands according to their relevant quantum numbers and properties. The existence of helical carriers with a linear dispersion offers a test bed for the studies of the fundamental massless Dirac fermions and antifermions.

This work has been supported by the excellence cluster The Hamburg Centre for Ultrafast Imaging—Structure, Dynamics and Control of Matter at the Atomic Scale of the Deutsche Forschungsgemeinschaft (Grant No. EXC-1024). We thank M. I. Katsnelson, D. Pfannkuche, and A. Lichtenstein for fruitful discussions. R. H. B. likes to thank Klaus von Klitzing for discussions.

J. S. and M. P. contributed equally to this work.

[1] C. L. Kane and E. J. Mele, Phys. Rev. Lett. **95**, 226801 (2005).
[2] C. L. Kane and E. J. Mele, Phys. Rev. Lett. **95**, 146802 (2005).
[3] M. Z. Hasan and C. L. Kane, Rev. Mod. Phys. **82**, 3045 (2010).
[4] H. Min, J. E. Hill, N. A. Sinitsyn, B. R. Sahu, L. Kleinman, and A. H. MacDonald, Phys. Rev. B **74**, 165310 (2006).
[5] Y. Yao, F. Ye, X.-L. Qi, S.-C. Zhang, and Z. Fang, Phys. Rev. B **75**, 041401 (2007).
[6] S. Konschuh, M. Gmitra, and J. Fabian, Phys. Rev. B **82**, 245412 (2010).
[7] M. I. Katsnelson, *Graphene: Carbon in Two Dimensions* (Cambridge University Press, Cambridge, England, 2012).
[8] A. H. C. Neto, F. Guinea, N. M. R. Peres, K. S. Novoselov, and A. K. Geim, Rev. Mod. Phys. **81**, 109 (2009).
[9] A. K. Geim and K. S. Novoselov, *Nanoscience and Technology: A Collection of Reviews from Nature Journals* (World Scientific, Singapore, 2010), pp. 11–19.
[10] M. O. Goerbig, Rev. Mod. Phys. **83**, 1193 (2011).
[11] G. P. Mikitik and Y. V. Sharlai, Phys. Rev. Lett. **82**, 2147 (1999).
[12] H. Suzuura and T. Ando, Phys. Rev. Lett. **89**, 266603 (2002).
[13] M. I. Katsnelson, K. Novoselov, and A. K. Geim, Nat. Phys. **2**, 620 (2006).

[14] M. I. Katsnelson, Eur. Phys. J. B **51**, 157 (2006).
[15] E. V. Gorbar, V. P. Gusynin, V. A. Miransky, and I. A. Shovkovy, Phys. Rev. B **66**, 045108 (2002).
[16] M. Gmitra, S. Konschuh, C. Ertler, C. Ambrosch-Draxl, and J. Fabian, Phys. Rev. B **80**, 235431 (2009).
[17] See Supplemental Material at http://link.aps.org/supplemental/10.1103/PhysRevLett.122.046403 for information regarding sample fabrication, characterization, and theoretical concepts, which includes Refs. [18–26].
[18] Graphenea, 2019, https://www.graphenea.com/collections/buy-graphene-films.
[19] X. Liang, B. A. Sperling, I. Calizo, G. Cheng, C. A. Hacker, Q. Zhang, Y. Obeng, K. Yan, H. Peng, Q. Li, X. Zhu, H. Yuan, A. R. Hight Walker, Z. Liu, L.-m. Peng, and C. A. Richter, ACS Nano **5**, 9144 (2011).
[20] K. Nagashio, T. Yamashita, T. Nishimura, K. Kita, and A. Toriumi, J. Appl. Phys. **110**, 024513 (2011).
[21] M. Her, R. Beams, and L. Novotny, Phys. Lett. A **377**, 1455 (2013).
[22] W. Han, R. K. Kawakami, M. Gmitra, and J. Fabian, Nat. Nanotechnol. **9**, 794 (2014).
[23] F. D. M. Haldane, Phys. Rev. Lett. **61**, 2015 (1988).
[24] F. Guinea, M. I. Katsnelson, and M. A. H. Vozmediano, Phys. Rev. B **77**, 075422 (2008).
[25] T. O. Wehling, A. V. Balatsky, A. M. Tsvelik, M. I. Katsnelson, and A. I. Lichtenstein, Europhys. Lett. **84**, 17003 (2008).
[26] N. Gu, M. Rudner, A. Young, P. Kim, and L. Levitov, Phys. Rev. Lett. **106**, 066601 (2011).
[27] K. S. Novoselov, A. K. Geim, S. V. Morozov, D. Jiang, M. I. Katsnelson, I. V. Grigorieva, S. V. Dubonos, and A. A. Firsov, Nature (London) **438**, 197 (2005).
[28] R. G. Mani, J. Hankinson, C. Berger, and W. A. de Heer, Nat. Commun. **3**, 996 (2012).
[29] T. J. Lyon, J. Sichau, A. Dorn, A. Centeno, A. Pesquera, A. Zurutuza, and R. H. Blick, Phys. Rev. Lett. **119**, 066802 (2017).
[30] T. J. Lyon, J. Sichau, A. Dorn, A. Zurutuza, A. Pesquera, A. Centeno, and R. H. Blick, Appl. Phys. Lett. **110**, 113502 (2017).
[31] E. I. Rashba, Phys. Rev. B **79**, 161409 (2009).
[32] P. M. Platzman and P. A. Wolff, *Waves and Interactions in Solid State Plasmas* (Academic Press, New York, 1973), Vol. 13.
[33] C. P. Slichter, *Principles of Magnetic Resonance*, Springer Series in Solid-State Sciences (Springer, Berlin, 1990), Vol. 1.
[34] E. McCann, K. Kechedzhi, V. I. Falko, H. Suzuura, T. Ando, and B. L. Altshuler, Phys. Rev. Lett. **97**, 146805 (2006).
[35] R. Winkler and H. Deshpande, Phys. Rev. B **95**, 235312 (2017).
[36] J. C. Boettger and S. B. Trickey, Phys. Rev. B **75**, 121402 (2007).